Technical Memorandum NESS 72

RADIATION BUDGET DATA FROM THE METEOROLOGICAL SATELLITES, ITOS 1 AND NOAA 1

Donald H. Flanders and William L. Smith

Washington, D.C.
August 1975

noaa NATIONAL OCEANIC AND ATMOSPHERIC ADMINISTRATION / National Environmental Satellite Service

NOAA TECHNICAL MEMORANDUMS

National Environmental Satellite Service Series

The National Environmental Satellite Service (NESS) is responsible for the establishment and operation of the environmental satellite systems of NOAA.

NOAA Technical Memorandums facilitate rapid distribution of material that may be preliminary in nature and so may be published formally elsewhere at a later date. Publications 1 through 20 and 22 through 25 are in the earlier ESSA National Environmental Satellite Center Technical Memorandum (NESCTM) series. The current NOAA Technical Memorandum NESS series includes 21, 26, and subsequent issuances.

Publications listed below are available from the National Technical Information Service, U.S. Department of Commerce, Sills Bldg., 5285 Port Royal Road, Springfield, Va. 22151. Prices on request. Order by accession number (given in parentheses). Information on memorandums not listed below can be obtained from Environmental Data Service (D831), 3300 Whitehaven St., NW., Washington, D.C. 20235.

NESS 33 Use of Satellite Data in East Coast Snowstorm Forecasting. Frances C. Parmenter, February 1972, 21 pp. (COM-72-10482)

NESS 34 Chromium Dioxide Recording--Its Characteristics and Potential for Telemetry. Florence Nesh, March 1972, 10 pp. (COM-72-10644)

NESS 35 Modified Version of the Improved TIROS Operational Satellite (ITOS D-G). A. Schwalb, April 1972, 48 pp. (COM-72-10547)

NESS 36 A Technique for the Analysis and Forecasting of Tropical Cyclone Intensities From Satellite Pictures. Vernon F. Dvorak, June 1972, 15 pp. (COM-72-10840)

NESS 37 Some Preliminary Results of 1971 Aircraft Microwave Measurements of Ice in the Beaufort Sea. Richard J. DeRycke and Alan E. Strong, June 1972, 8 pp. (COM-72-10847)

NESS 38 Publications and Final Reports on Contracts and Grants, 1971. NESS, June 1972, 7 pp. (COM-72-11115)

NESS 39 Operational Procedures for Estimating Wind Vectors From Geostationary Satellite Data. Michael T. Young, Russell C. Doolittle, and Lee M. Mace, July 1972, 19 pp. (COM-72-10910)

NESS 40 Convective Clouds as Tracers of Air Motion. Lester F. Hubert and Andrew Timchalk, August 1972, 12 pp. (COM-72-11421)

NESS 41 Effect of Orbital Inclination and Spin Axis Attitude on Wind Estimates From Photographs by Geosynchronous Satellites. Linwood F. Whitney, Jr., September 1972, 32 pp. (COM-72-11499)

NESS 42 Evaluation of a Technique for the Analysis and Forecasting of Tropical Cyclone Intensities From Satellite Pictures. Carl O. Erickson, September 1972, 28 pp. (COM-72-11472)

NESS 43 Cloud Motions in Baroclinic Zones. Linwood F. Whitney, Jr., October 1972, 6 pp. (COM-73-10029)

NESS 44 Estimation of Average Daily Rainfall From Satellite Cloud Photographs. Walton A. Follansbee, January 1973, 39 pp. (COM-73-10539)

NESS 45 A Technique for the Analysis and Forecasting of Tropical Cyclone Intensities From Satellite Pictures (Revision of NESS 36). Vernon F. Dvorak, February 1973, 19 pp. (COM-73-10675)

NESS 46 Publications and Final Reports on Contracts and Grants, 1972. NESS, April 1973, 10 pp. (COM-73-11035)

NESS 47 Stratospheric Photochemistry of Ozone and SST Pollution: An Introduction and Survey of Selected Developments Since 1965. Martin S. Longmire, March 1973, 29 pp. (COM-73-10786)

NESS 48 Review of Satellite Measurements of Albedo and Outgoing Long-Wave Radiation. Arnold Gruber, July 1973, 12 pp. (COM-73-11443)

NESS 49 Operational Processing of Solar Proton Monitor Data. Louis Rubin, Henry L. Phillips, and Stanley R. Brown, August 1973, 17 pp. (COM-73-11647/AS)

(Continued on inside back cover)

NOAA Technical Memorandum NESS 72

RADIATION BUDGET DATA FROM THE METEOROLOGICAL SATELLITES, ITOS 1 AND NOAA 1

Donald H. Flanders and William L. Smith

Washington, D.C.
August 1975

UNITED STATES
DEPARTMENT OF COMMERCE
Rogers C. B. Morton, Secretary

NATIONAL OCEANIC AND
ATMOSPHERIC ADMINISTRATION
Robert M. White, Administrator

National Environmental
Satellite Service
David S. Johnson, Director

NOAA Technical Memorandum NESS 72

RADIATION BUDGET DATA FROM THE METEOROLOGICAL SATELLITES, ITOS 1 AND NOAA 1

Donald H. Flanders and William L. Smith

Washington, D.C.
August 1975

CONTENTS

RADIATION BUDGET DATA FROM THE METEOROLOGICAL SATELLITES,[1] ITOS 1 AND NOAA 1

Donald H. Flanders[2] and William L. Smith[3]
NOAA, Washington, D.C.

ABSTRACT. The procedures used to process the Flat Plate Radiometer data from the two satellites are described. The results are presented for the periods of good data acquisition: 23 March through 25 June 1970 for ITOS 1 and 18 February through 16 March and 10 May through 27 May 1971 for NOAA 1. For the common observation month of May in 1970 and 1971, no significant variation in globally averaged albedo was observed. The mean values of outgoing long-wave flux (518 ly/day) are in agreement with prior observations from ESSA, Nimbus, and Meteor satellites. The derived planetary albedo values are higher than prior observations, possibly because the ITOS and NOAA observations were made at local times when convective cloudiness over land is most intense.

I. INTRODUCTION

NOAA 1 and ITOS 1 carried omnidirectional Flat Plate Radiometers (FPRs)[4] for measuring the outgoing radiation from Earth and the atmosphere. Black and white sensors are used to observe respectively the short-wavelength (0.2- to 4.0-μm) and long-wavelength (4- to 40-μm) components of the outgoing flux of radiation at satellite altitude. The flux, formed by the integral over 2π sr of radiance components impinging on the flat plate sensor, emanates from an Earth area several thousand kilometers across. The spatial resolution of these data is considered sufficient for estimating certain large-scale features of the Earth's radiation budget (e.g., the mean monthly zonal and meridional radiation profiles and the time and space variation of mean monthly albedo, long-wave flux, and net radiation on the scale of continents and oceans). The net planetary radiation budget value derived by global integration of the low-resolution FPR data is, in principle, limited only by the sampling characteristics of the satellite's orbit.

In this memorandum, the procedures used to process the ITOS-1 and NOAA-1 FPR data are given. The results are presented for the periods of good data acquisition. These periods were 23 March through 25 June 1970 for ITOS 1 and 18 February through 16 March and 10 May through 27 May 1971 for NOAA 1.

The ITOS-1 and NOAA-1 FPRs were developed by the University of Wisconsin at Madison. The university's instruments also were flown on ESSA 3, 5, and 7, which were spinning satellites.[5] The data from these earlier experiments have been processed by both the University of Wisconsin (Suomi et al. 1967) and the National Environmental Satellite Service (MacDonald 1970).

The ITOS-1 and NOAA-1 FPRs, like those on the ESSA satellites, experienced degradation in orbit. Since there was no on-board calibration facility for these instruments,

---

[1] Improved TIROS Operational Satellite (ITOS); Television Infrared Observation Satellite (TIROS); National Oceanic and Atmospheric Administration (NOAA)

[2] Office of Management and Computer Systems

[3] National Environmental Satellite Service (NESS)

[4] There were two types of FPRs on these two satellites, a Radiative Equilibrium Sensor and a Thermal Feedback Sensor. Difficulties were encountered in attempting to process the Thermal Feedback Sensor data; thus this memorandum deals solely with the processing of the Radiative Equilibrium FPR data.

[5] Environmental Science Services Administration (ESSA)

certain assumptions about the Earth's radiative properties were necessary to obtain meaningful radiation values from the raw data output of the FPRs. In processing the spinning ESSA satellite's FPR data, one assumption was that the Net Planetary Radiation (NPR) was zero when integrated over a period of several days. Another assumption also was necessary--no discontinuity in the meridional gradient of outgoing long-wave radiation as the ESSA satellite moved from darkness to daylight (MacDonald 1970). ITOS 1 and NOAA 1 were stabilized by three axes so that the FPR always faced Earth. As a consequence, the data-processing procedures differ from those for the spinning FPR. The following decision was reached--not to impose the zero NPR assumption for calibration of the NOAA FPR data because it is unlikely to hold for the Earth over short periods especially because the sampling was at only two local times (3 a.m. and 3 p.m.) for ITOS 1 and NOAA 1.

II. PHYSICAL BASIS OF THE MEASUREMENT

The FPR measurement of radiation flux is based on the radiative equilibrium principle [i.e., an absorbing (and emitting) body suspended in space will assume a temperature equal to that of another emitting (and absorbing) body surrounding it]. If the FPR were a perfect black body completely isolated from its surroundings (i.e., the spacecraft) and the Earth were the only source of radiation, then the flux of radiation leaving the Earth-atmosphere system would be related directly to temperature of the FPR by the Stefan-Boltzmann law. Of course, the FPR is not such a perfectly absorbing radiation sensor; and it is not suspended in space but is in thermal contact with a spacecraft. Consequently, the relationship between the equilibrium temperature of the FPR and the Earth radiation flux sensed is more complicated.

A full description of the FPR is given by Nelson and Parent (1967). The sensor consists of two, plane surface disks (one black and one white) exposed to radiation within 2π sr about the disk normal (the satellite nadir). The black disk is a good absorber of both long-wave and short-wave radiation; the white disk is a good absorber of the long-wave radiation component but is a strong reflector of the short-wave radiation. The use of the black and white disks enables one to distinguish between Earth-emitted long-wave radiation and Earth-reflected short-wave radiation. The device is shielded from radiation emitted by the spacecraft. The disks are suspended by thin threads to minimize conduction; however, the heat transfer by conduction must be taken into account. A thermistor is used for measuring the temperature of the disks and the disk mounts. Knowing the thermal conductivity of the threads that suspend the disks permits determination of the conductive heat exchange. The heat loss by radiation can be determined readily if the emissivity and temperature of the disks are known. Finally, the thermal heat capacity and rate of change of disk temperature must be known to account for the time rate of change of stored heat.

III. CALIBRATION OF THE FPR DATA

A. General Considerations

Earth radiation flux values from the FPR-sensing disk temperature observations are determined through solution of heat balance equations for black and white sensors. The heat balance equations are:

$$\alpha_{s,j} S + \alpha_{r,j} R + \alpha_{l,j} L = \varepsilon_j \sigma T_j^4 + c_j (T_j - T_m) + K \frac{\partial T_j}{\partial t} \qquad (1)$$

where

S ≡ direct solar irradiance on the disk,

R ≡ Earth-reflected solar irradiance on the disk,

L ≡ Earth-emitted irradiance on the disk,

j ≡ sensor type (b or w for black or white),

$\alpha_{s,j}$ ≡ absorptivity of the disk for direct solar radiation,

$\alpha_{r,j}$ ≡ absorptivity of the disk for reflected solar radiation,

$\alpha_{l,j}$ ≡ absorptivity of the disk for emitted long-wave radiation,

ε_j ≡ emissivity of the disk,

σ ≡ Stefan-Boltzmann constant,

T_j ≡ disk temperature,

c_j ≡ coefficient of heat conduction from the sensing disk to its mounting,

T_m ≡ temperature of the sensor mount,

K_j ≡ disk heat capacitance coefficient, and

t ≡ time.

Obtaining useful estimates of the Earth radiation components when there is direct solar radiation on the sensors was found to be difficult because, in this case, the term $\alpha_{s,j} S$ in eq (1) is much larger than the $(\alpha_{r,j} R + \alpha_{l,j} L)$ term. Also, the dependence on α_s on solar incidence angle is not well known. As a consequence, data were not processed during periods of direct solar illumination. This constraint caused gaps in the long-wave radiation during the night for areas extending over 30° of latitude in the winter hemisphere.

If one neglects data when $S \neq 0$ and divides by $\alpha_{l,j}$, eq (1) becomes

$$\alpha'_j R + L = \varepsilon'_j \sigma T_j^4 + c'_j (T_j - T_m) + K'_j \frac{\partial T_j}{\partial t} \qquad (2)$$

where the prime denotes division by $\alpha_{l,j}$. In processing the data, one must assume values for the coefficients of eq (2). Values for c_j and K_j were determined from calibration tests by the University of Wisconsin. In MacDonald (1970), an assumption on the basis of prior inflight experience was that the ratio of emissivity to absorptivity of the black sensing disk for long-wave radiation (i.e., ε'_b) was invariant throughout the life of the sensor (i.e., any degradation of the black paint results in a proportional change in emissivity and absorptivity). In like manner, another assumption was that any change of the absorptivity of the black sensing disk for reflected short-wave radiation was proportional to a change in its absorptivity for long-wave radiation (i.e., α'_b is constant). The values of the assumed constants, based upon calibration data provided by the University of Wisconsin, are given in table 1.

The coating used on the white sensing disk is known to degrade in orbit (House 1965, MacDonald 1970). Consequently, the values of the coefficients α' and ε' for the white sensor were defined from in-flight data in the subsequent described manner. Once these coefficients were defined, the long-wave and reflected radiation components of the flux of radiation from the Earth at satellite altitude were calculated from the simultaneous solution of eq (2). For daytime conditions,

Table 1.--Values of the coefficients assumed to be invariant in orbit*

	ITOS 1		NOAA 1	
	Black	White	Black	White
α'_j	1.055	Variable	1.081	Variable
ε'_j	0.98	Variable	0.98	Variable
c'_j	.000888	0.001080	.000917	0.001080
K'_j	.00337	.00395	.00348	.00395

*Units of c_j and K_j are cal/(cm^2 °C min) and cal/(cm^2 °C), respectively.

Note that variations in $\alpha_{l,j}$ will produce small variations in c'_j and K'_j; however, since the terms involving c'_j and K'_j are relatively small, such variations can be neglected.

$$R = 0, \qquad (3a)$$

$$L = \frac{\alpha'_w E_b - \alpha'_b E_w}{\alpha'_w - \alpha'_b}, \qquad (3b)$$

and

$$R = \frac{E_w - E_b}{\alpha'_w - \alpha'_b}. \qquad (3c)$$

For nighttime conditions,

$$L = \frac{E_b + E_w}{2} \qquad (3d)$$

and

$$R = 0. \qquad (3e)$$

In eq (3),

$$E_j = \varepsilon'_j \sigma T_j^4 + c'_j (T_j - T_m) + K'_j \frac{\partial T_j}{\partial t} \qquad (4)$$

where T_j, T_m, and $\partial T_j / \partial t$ are evaluated from the thermistor outputs obtained once every minute.

B. In-Flight Determination of the Absorptivity-Emissivity Coefficients for the White Disk

Values for the coefficients ε'_w and α'_w were determined daily. The specification of ε'_w was straightforward using nighttime observations of E_w and E_b. From eq (2), at night when $R = 0$,

$$\varepsilon'_w = \frac{E_b - c'_w (T_w - T_m) - K'_w (\partial T_w / \partial t)}{\sigma T_w^4} \qquad (5)$$

where E_b has been defined by eq (4). The average value of ε'_w, determined from all the nighttime observations over a 24-hr period, was used to process all the daytime observations for the same 24-hr period.

To determine α'_w, one must impose some assumption about the Earth's radiative field. For example, MacDonald (1970) assumed that the net planetary radiation is equal to zero over short periods of time (e.g., a week or less). Since this did not seem to be a reasonable assumption, considering the time and space bias of the observations obtained from a single satellite, another more realistic assumption was desired. On the basis of comparisons between 30-day mean values of daytime and nighttime infrared radiation observations from the scanning radiometers aboard the NOAA satellites, there was no significant systematic difference between daytime and nighttime values of outgoing long-wave radiation over tropical oceanic regions (Winston 1975). As a result of this finding, an assumption was that, over a period of 7 days, the mean long-wave radiation flux reaching the FPR from the tropical oceans (30°N to 30°S) was the same both by night and by day. Equation (3b), written separately for daytime and nighttime values and equated to eliminate L, yields the solution

$$\alpha'_w = \alpha'_b \left(\frac{\tilde{E}_w - \bar{E}_w}{\tilde{E}_b - \bar{E}_b} \right) \qquad (6)$$

where $\tilde{E}_w$ and $\tilde{E}_b$ are average daytime values of E [from eq (4)] for the white and black disks and $\bar{E}_w$ and $\bar{E}_b$ are average nighttime values for the 7-day period.

Figures 1A and 1B show the variation of ε'_w and α'_w obtained for the ITOS-1 and NOAA-1 FPRs, respectively, for the periods of useable data. The short-term fluctuations are noise attributable to insufficient data for defining accurate mean energy values to compute ε'_w and α'_w. The white sensor on ITOS 1 apparently degraded significantly over a 3-mo period of observation; this is indicated by the increase in ε'_w (because of a decrease in long-wave absorptivity) and α'_w (because of a decrease in the short-wave reflectivity of the coating of the white disk). For NOAA 1, the time variation was somewhat different in that there was no significant change in the ratio of long-wave emissivity to absorptivity of the white disk but a significant degradation in the reflectivity (increase in absorptivity) of the white disk to Earth-reflected short-wave radiation (i.e., α'_w increased for 0.36 to about 0.42 between February and May 1971).

C. Additional Considerations

Having defined all the coefficients needed to calculate E_b and E_w using eq (4) as well as α'_w and α'_b, one computes L and R every minute through the satellite orbit. (ITOS 1 and NOAA 1 travel about 900 km in 1 min.) To reference the fluxes observed at satellite altitude (1460 km) to the flux at the effective "top of the atmosphere" (10 km), one must assume that the Earth's radiation field was isotropic. This assumption is, of course, not generally valid; but it enables one to account for *systematic* differences in the measurements of flux due to the geometry of the measurement (i.e., the sensor altitude). The geometrical relationship between the flux of isotropic radiation from the Earth, observed by a flat plate sensor at a reference altitude h_0 with respect to that observed at a satellite altitude h_s, is

$$F_0 = \left(\frac{r + h_s}{r + h_0} \right)^2 \text{ and } F_s = CF_s \qquad (7)$$

where F is the flux of isotropic Earth radiation, r is the radius of the Earth, and C is a geometric constant. For ITOS 1 and NOAA 1, C is approximately 1.51.

The values of Earth-reflected radiation are converted to albedo [eq (4)] using the relation

$$A = R/I. \qquad (8)$$

I, the incoming solar irradiance, is given by

$$I = S_0 \cos \theta_0 / \rho^2 \qquad (9)$$

where S_0 is the solar constant, assumed to be 2794 ly/day (Drummond 1970, Thekaekara and Drummond 1971), θ_0 is the solar zenith angle at the centroid of the illuminated Earth area, and ρ is the Earth-Sun distance in units of its mean. The Earth location of the centroid of the illuminated area, which is used to compute θ_0 and to locate A geographically, is obtained in the same manner given by MacDonald (1970).

The "net radiation" N is obtained by the relation

$$N = I - R - L = (1 - A)I - L. \qquad (10)$$

IV. RESULTS

Figures 2, 3, and 4 show maps of outgoing long-wave radiation flux and albedo derived from ITOS-1 FPR data for the months of April, May, and June 1970, respectively. These maps were produced by means of a

standard objective analysis program utilizing a numerical grid with a 5° x 5° latitude-longitude mesh. Since the Earth area from which 90% of the radiation sensed by the FPR observation originates has a radius of 7.5°, each observation was allowed to influence all grid points within 7.5° of great circle distance from the satellite subpoint at the time of measurement. This was accomplished by weighting the observation assigned to the various grid points by a value proportional to the inverse square of the distance of the grid point from the satellite subpoint. This analysis procedure appears to give better definition to highs and lows than when the observation was assigned only to the grid point nearest the satellite subpoint.

The maps presented here are similar to those obtained from radiation budget measurements from prior satellites (Winston and Taylor 1967, Raschke and Bandeen 1970, Vonder Haar and Suomi 1971, Vonder Haar et al. 1972). Most of the cellular features of the long-wave radiation and albedo patterns are produced by cloudiness because centers of high albedo correspond to centers of low outgoing long-wave radiation. The most notable exception to this characteristic is found over Northern Africa where there is a maximum of both outgoing long-wave radiation and albedo because of its warm and bright desert surface. The most intense zonal gradient of radiation is found over India; this zone intensifies dramatically over the 3-mo period, possibly because of the concurrent development of the summer monsoon. Another time variation is the northward shift of the center of low outgoing radiation from northern South America into the Caribbean. Since the center of high albedo remains stationary over South America, this northward shift may be due to the increase in cirrus clouds over the Caribbean, which would affect the outgoing long-wave flux more than the albedo. Also interesting are the development of a large ridge of outgoing long-wave radiation over the west-central part of the United States and a trough off the east coast. In this case, however, the albedo pattern remains nearly zonal over the 3-mo period. This feature probably is due to the relatively large increase in the surface temperature of the continental United States and little change in cloudiness throughout the spring months.

Figure 5 shows the net radiation patterns for April, May, and June 1970. The only zonal features that stand out, because of the low geographical resolution of the FPR data, are the subtropical high radiation sources and Sahara radiation sink, both of which change considerably throughout the Northern Hemisphere spring season.

Figures 6, 7, and 8 show the long-wave radiation, albedo, and net radiation patterns, respectively, derived from the NOAA-1 FPR data for 18 February through 16 March and 10 May through 27 May 1971. There are some notable differences between the patterns of May 1970 with those of May 1971; however, many of these differences may not be real but may be due only to differences in observation patterns of ITOS 1 and NOAA 1. The geographical distributions of the population of both day and night long-wave observations and albedo are presented in figures 9, 10, and 11. Comparison of figure 3 with figures 6B and 7B shows that the zonal gradients of long-wave radiation and albedo in the tropical latitudes are much stronger for May 1971. Note also the more intense low long-wave radiation center over South America; however, the population maps in figures 9 and 10 show much greater gaps in the NOAA satellite coverage for May 1971 than in the ITOS satellite coverage for May 1970. The difference in the long-wave radiation low center over South America is probably due to the fact that, for May 1970, this feature was derived from an average of the day and night ITOS observations while, for May 1971, it was derived only from daytime NOAA observations. (See fig. 10B.) Since convective cloudiness is responsible for the outgoing long-wave radiation minimum, that the NOAA-1 daytime observations reveal a more intense minimum than the ITOS-1 day and night observations is not surprising. Also note that, in May 1971, there is an intense radiation low over the Gold Coast of Africa; in May 1970, there is only weak evidence of this feature. Here, again, figures 10 and 11 show that this area is a region of relatively few daytime and nighttime observations for NOAA 1; however, this feature is real (see the subsequent text) and may have propagated from the interior of South Africa. (See fig. 6A.) The net radiation fields (fig. 8) show that the relative deficit of radiation over the Sahara Desert is much less intense during the February-March period. Although this might be expected because of lower surface temperatures (outgoing long-wave radiation) during the winter months, much of this difference may be due to the lack of useable NOAA-1 nighttime observations over the Sahara during May.

Figure 12 shows the outgoing long wave radiation flus patterns for May 1971 obtained from the NOAA-1 high resolution Scanning Radiometer (SR). The flux values were estimated from the SR 11-μm window-channel radiances using regression relationships derived from theoretical computations of total flux and 11-μm radiance. The instantaneous resolution of the SR is 4 n.mi.

at nadir; but in this presentation, the values have been averaged over areas of 5° of latitude by 5° of longitude. Comparisons between figure 12 and figure 6B show good correspondence between the large-scale features of the flux patterns derived from the observations obtained by the FPR and SR sensors. Examples are the ridge of high values over Canada, the low center over South America, the high values associated with the subtropical high pressure regions, the intense gradient over India, and the intense low center over the Gold Coast of Africa. The differences between the two patterns are caused by the differences in resolution of the two sensors. The low resolution of the FPR drastically smooths the true Earth outgoing flux pattern. Note that the FPR is incapable of resolving the intensities of the low and high radiation centers and of the band of minimum outgoing radiation flux near the Equator (EQ) because of the cloudiness associated with the intertropical convergence zone. The inherent smooth representation of the true Earth outgoing flux field is the major deficiency of FPR flux measurements at satellite altitudes.

Figures 13 and 14 present profiles of the zonally averaged radiation parameters. Comparing May 1970 with May 1971 (fig. 14), one finds generally good correspondence between the zonal mean outgoing long-wave flux in the Southern Hemisphere and the albedo in the Northern Hemisphere. South of 20°S, however, the albedo for May 1971 is higher than that of 1970; however, only a minor difference in the net outgoing radiation for the 2 yr between 20°S and 40°S results because of compensatory differences in the long-wave radiation for the 2 yr. The zonal mean values of net radiative heating appear to be slightly greater for May 1971 than for May 1970; however, these differences may not be significant since they may reflect only differences at the 3 a.m. and 3 p.m. sampling times. This difference in net radiation is mainly due to long wave radiation measurements tending to be higher during May 1971 than during May 1970 in most latitude zones; this indicates that this net radiation difference is due to deficiencies in the calibration of the ITOS and NOAA FPR instruments rather than to a real difference in the atmospheric radiation budget.

Finally, table 2 presents global average values (weighted by area) of the radiation budget parameters. There is excellent correspondence between the globally averaged albedo values for the 2 yr, with the planetary albedo generally decreasing between February and June. Both the ITOS-1 and NOAA-1 measurements also indicate a very slight decrease in outgoing long wave radiation flux, the net result being an increase in the net radiation gained by the Earth-atmosphere system; however, the 3% relative difference indicated in the outgoing long-wave flux for the 2 yr is not believed to be real. The differences most likely are due to uncertainties in the values assumed for the various emissivity, conductivity, and heat-capacity coefficients used for calibrating the FPR data.

Table 2.--Global average values of albedo, long-wave, and net incoming radiation

Satellite	Albedo	Long-wave flux	Net flux
ITOS 1 (1970)	(%)	(ly/day)	(ly/day)
Apr.	34.8	525.4	-54
May	34.1	525.2	-68
June	33.3	524.5	-73
NOAA 1 (1971)			
Feb.-Mar.	35.1	510.0	-25
May	34.4	509.6	-54

The planetary albedo values derived from the ITOS-1 and NOAA-1 data are higher than those reported by Vonder Haar (1972) and others (∿34% vs. ∿30%). There is, however, agreement in the 2-yr average value of outgoing long-wave radiation (∿518 ly/day). Also, we note that the ITOS-1 and NOAA-1 observations both indicate a net loss of radiation on the planetary scale. Both the albedo discrepancy and the planetary radiation deficit might be due to the 3 p.m. local sampling time of the ITOS and NOAA orbit. The albedo tends to be a maximum in the middle and late afternoon because that is the period of maximum convective cloudiness over land; however, the total outgoing long-wave radiation does not decrease at the same rate as the albedo increases because of the corresponding increase in the surface temperature as convective cloudiness increases during the afternoon hours. In fact, comparison of monthly mean nighttime and daytime (3 a.m. and 3 p.m.) values of outgoing long-wave radiation over areas of extensive daytime convection (e.g., northern South America) indicated little diurnal variation. Consequently, the relatively high values of albedo that cause the net radiation deficit for the globe appear to be a result of the local sampling time of the satellite, which in this case is unrepresentative of mean daily conditions. If the actual planetary albedo value observed at 3 p.m. is 35%, this value represents a 17% increase over the previously observed daily

average of 30%. This result dramatically illustrates the need for representative diurnal sampling to estimate the planetary albedo and net radiation from satellite observations.

Table 2 also indicates that an assumption of zero net planetary radiation to calibrate the white sensor (which was made in the past) would have produced erroneous albedo results. If radiation balance had been assumed for the ITOS and NOAA sampling times, an erroneously low planetary albedo value of 26% would have resulted.

V. CONCLUSIONS

Radiation budget data were derived from the ITOS-1 and NOAA-1 FPR data. Unfortunately, there were only brief periods of good data acquisition from the two satellites. For the common observation month of May in 1970 and 1971, no significant variation in globally averaged albedo was observed, but there was a 3% decrease in the outgoing long-wave radiation observed between 1970 and 1971. This change is believed to be spurious because of the calibration uncertainties of the ITOS and NOAA FPR instruments. The 2-yr mean value of outgoing long-wave flux (518 ly/day) is, however, in agreement with prior observations from ESSA, Nimbus, and Meteor satellites (Vonder Haar et al. 1972). The derived planetary albedo values are higher than prior observations, presumably because the ITOS and NOAA observations were made at local times when convective cloudiness over land is most intense.

In the near future, highly improved (from an accuracy standpoint) Earth radiation budget data will be obtained from the Nimbus-F Earth Radiation Budget (ERB) experiment (Smith et al. 1975). In addition to wide-angle sensors for measuring total flux at satellite altitude, the ERB has high resolution scanning channels for observing the angular distribution of upwelling long-wave and short-wave radiance. From these measurements, fluxes of radiation can be obtained on the synoptic scale (500 km). Thus, to determine major regional sources and sinks of radiation and to assess their influence on the large scale and planetary radiation budget values obtained during the past decade with low-resolution plate and sphere sensors should be possible.

ACKNOWLEDGMENTS

We wish to thank J. S. Winston for his critical review of the manuscript as well as his helpful contributions. We acknowledge R. Boudreau and C. Beale for their contributions to development of FPR data-processing software. We thank L. Mannello and R. Ryan for their assistance in preparing this manuscript for publication and T. Schwier for typing it.

REFERENCES

Drummond, Andrew J., "Precision Radiometry and Its Significance in Atmospheric and Space Physics," *Advances in Geophysics*, Vol. 14, Academic Press, New York, N.Y., 1970, pp. 1-52.

House, F. B., "The Radiation Balance of the Earth From a Satellite," Ph. D. thesis, Department of Meteorology, The University of Wisconsin, Madison, 1965, 69 pp.

MacDonald, Torrence H., "Data Reduction Processes for Spinning Flat-Plate Satellite-Borne Radiometers," *ESSA Technical Report* NESC 52, National Environmental Satellite Center, Environmental Science Services Administration, U.S. Department of Commerce, Washington, D.C., July 1970, 37 pp.

Nelson, David F., and Parent, Robert, "The Prototype Flat Plate Radiometers for the ESSA III Satellite," *Studies in Atmospheric Energetics Based on Aerospace Probings*, Department of Meteorology, The University of Wisconsin, Madison, Mar. 1967, pp. 119-129.

Raschke, Ehrhard, and Bandeen, William R., "The Radiation Balance of the Planet Earth From Radiation Measurements of the Satellite Nimbus II," *Journal of Applied Meteorology*, Vol. 9, No. 2, Apr. 1970, pp. 215-238.

Smith, W. L., Hilleary, D. T., Jacobowitz, H., Howell, H. B., Hickey, J. R., and Drummond, Andrew J., "The Earth Radiation Budget (ERB) Experiment," *The Nimbus 6 User's Guide*, Goddard Space Flight Center, U.S. National Aeronautics and Space Administration, Greenbelt, Md., Feb. 1975, 227 pp.

Suomi, Verner E., Hanson, Kirby J., and Vonder Haar, Thomas H., "The Theoretical Basis for Low-Resolution Radiometer Measurements From a Satellite," *Studies in Atmospheric Energetics Based on Aerospace Probings*, Department of Meteorology, The University of Wisconsin, Madison, Mar. 1967, pp. 79-100.

Thekaekara, Matthew P., and Drummond, Andrew J., "Standard Values for the Solar Constant and Its Spectral Components," *Nature Physical Science*, Vol. 229, No. 1, Jan. 1971, pp. 6-9.

Vonder Haar, Thomas H., "Natural Variation of the Radiation Budget of the Earth-Atmosphere System as Measured From Satellites," *Preprints of the Conference on Atmospheric Radiation, Fort Collins, Colorado, August 7-9, 1972*, American Meteorological Society, Boston, Mass., 1972, pp. 211-220.

Vonder Haar, Thomas H., and Suomi, Verner E., "Measurement of the Earth's Radiation Budget From Satellites During a Five Year Period; Part 1: Extended Time and Space Means," *Journal of the Atmospheric Sciences*, Vol. 28, No. 3, Apr. 1971, pp. 305-314.

Vonder Haar, Thomas H., Raschke, Ehrhard, Pastenak, M., and Bandeen, William R., "The Radiation Budget of the Earth-Atmosphere System as Measured From the Nimbus-III Satellite (1969-70)," *Space Research XII*, Akademie-Verlag, Berlin, Germany, 1972, pp. 491-497.

Winston, J. S., National Environmental Satellite Service, National Oceanic and Atmospheric Administration, U.S. Department of Commerce, Washington, D.C., 1975 (personal communication).

Winston, J. S., and Taylor, V. Ray, "Atlas of World Maps of Long-Wave Radiation and Albedo--for Seasons and Months Based on Measurements From TIROS IV and TIROS VII," *ESSA Technical Report* NESC 43, National Environmental Satellite Center, Environmental Science Services Administration, U.S. Department of Commerce, Washington, D.C., Sept. 1967, 32 pp.

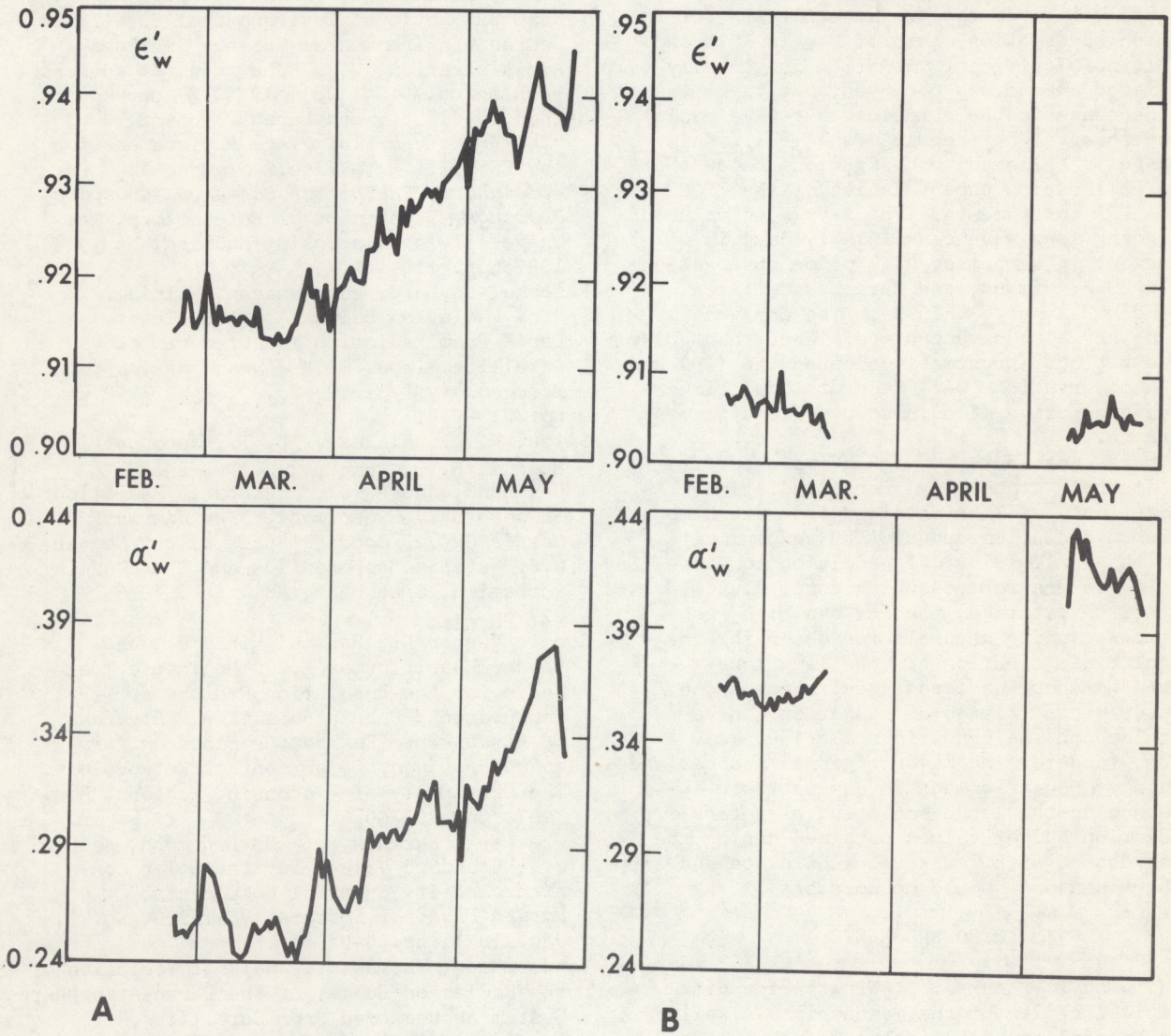

Figure 1.--Variation of ε'_w and α'_w obtained from FPRs aboard (A) ITOS 1 (1970) and (B) NOAA 1 (1971)

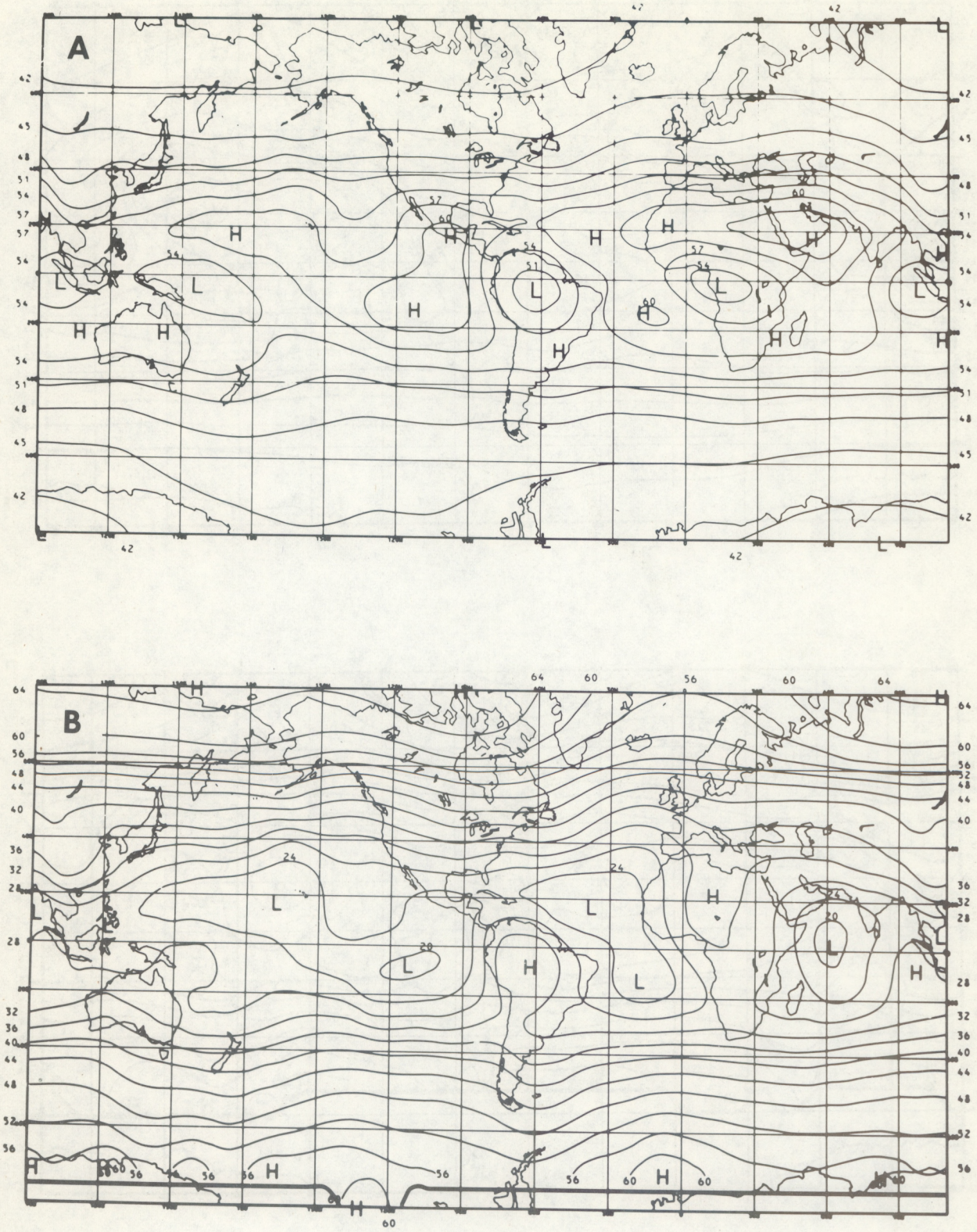

Figure 2.--Global analysis of measured outgoing long-wave radiation (A) and albedo (B) from the ITOS-1 FPR for April 1970. Long wave radiation values are in tens of langleys per day; albedo values are in percent.

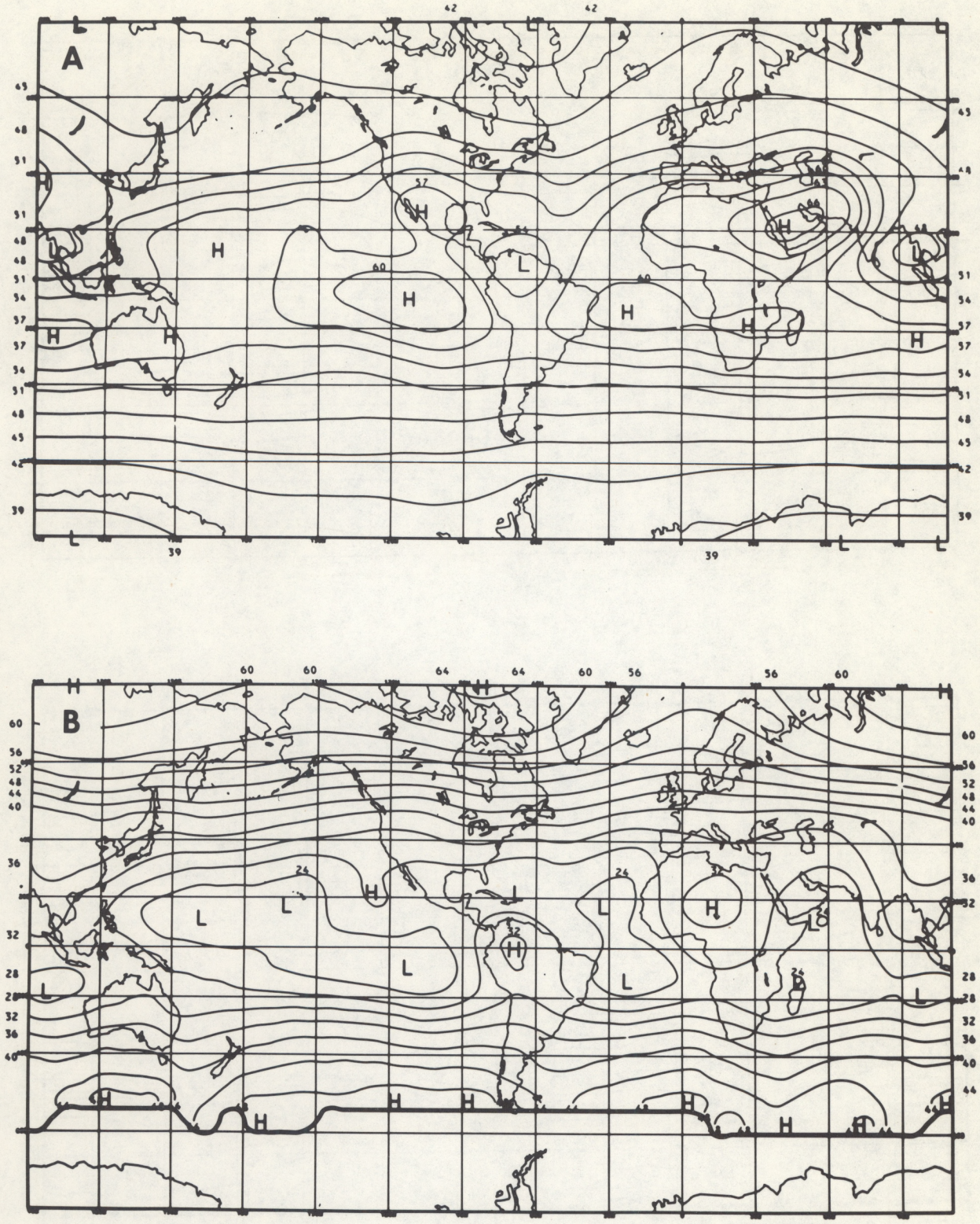

Figure 3.--Same as figure 2 except this is for May 1970.

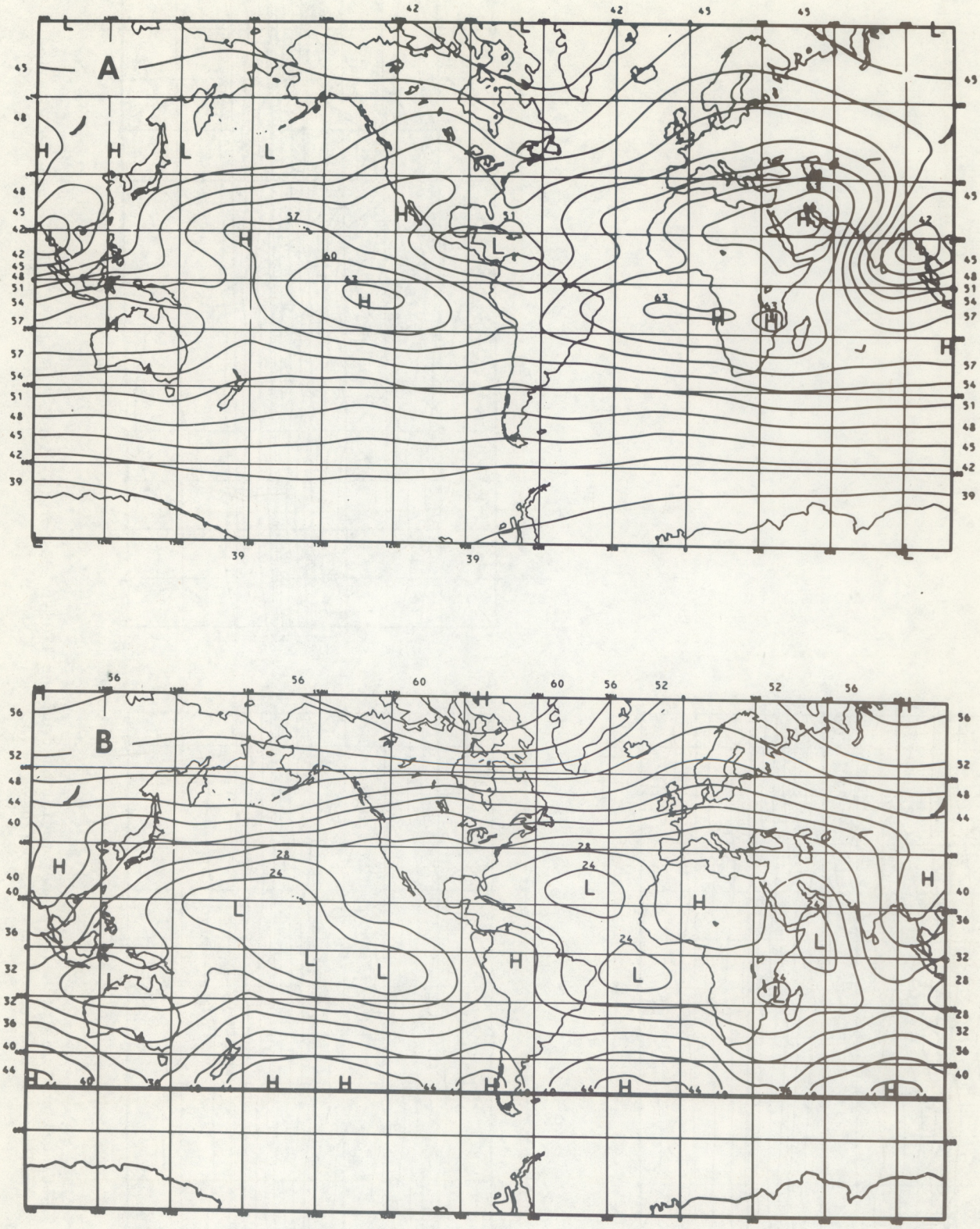

Figure 4.--Same as figure 2 except this is for June 1970.

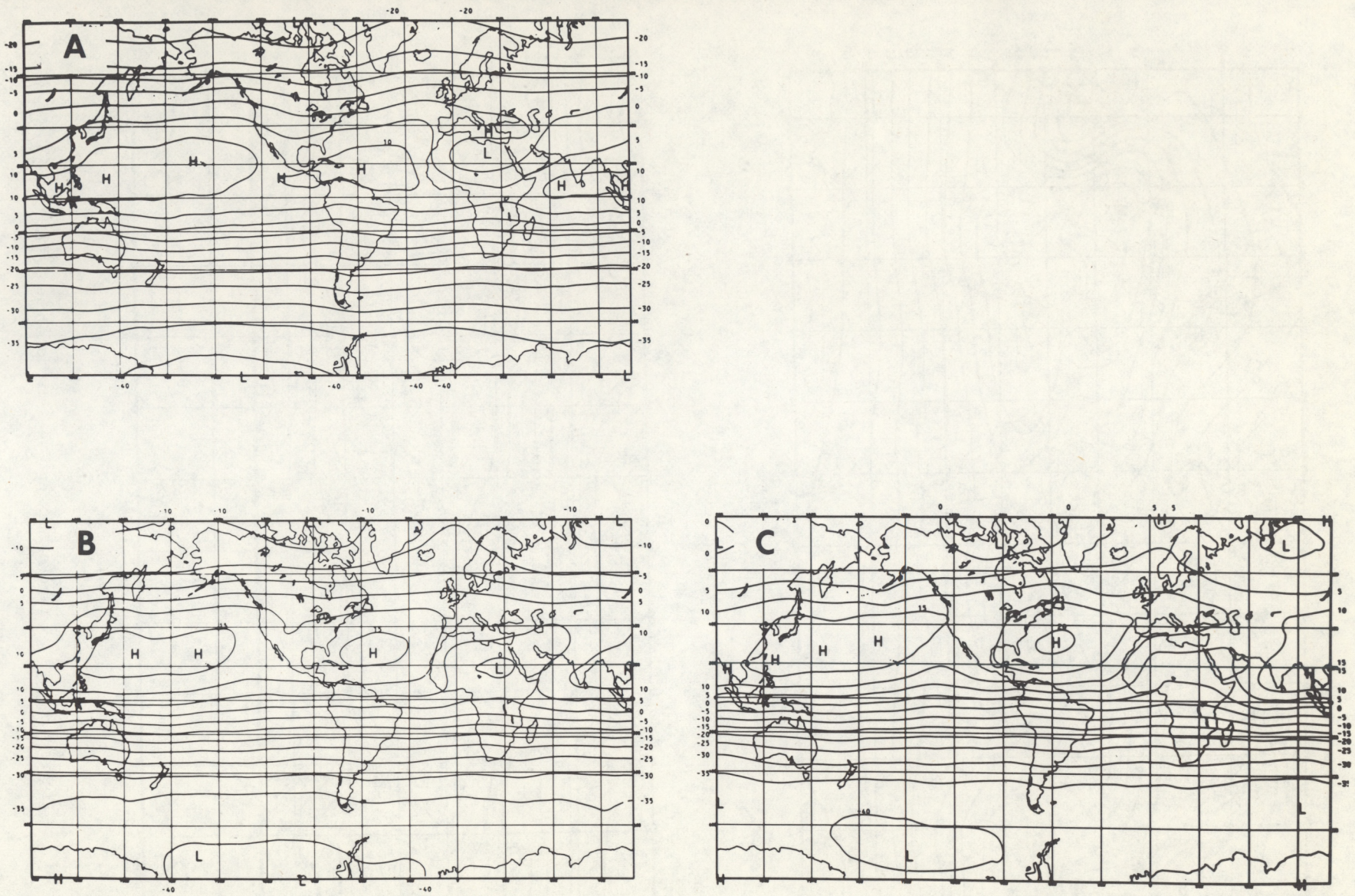

Figure 5.--Global analysis of measured net radiation from the ITOS-1 FPR for (A) April, (B) May, and (C) June 1970. The values are in tens of langleys per day.

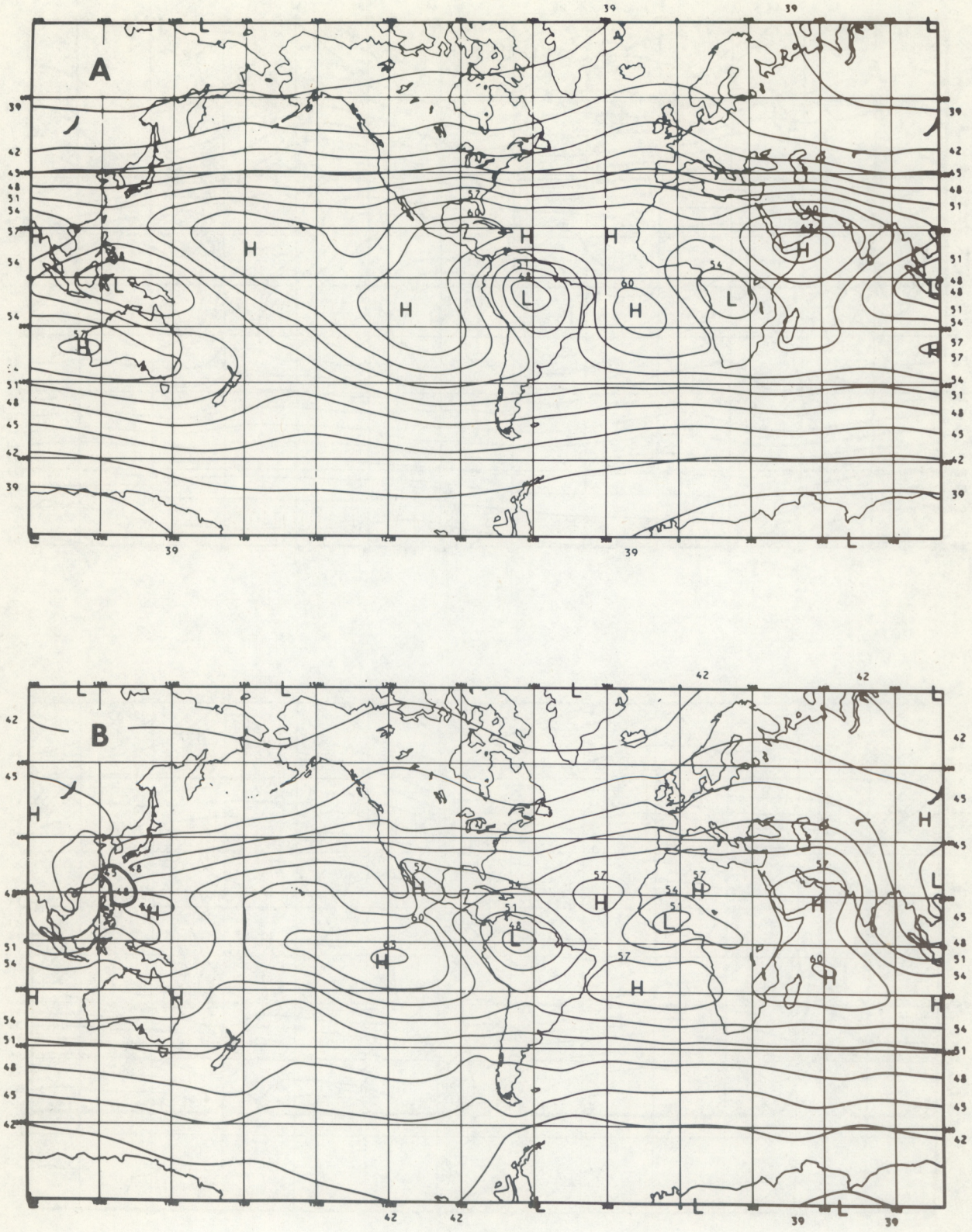

Figure 6.--Global analysis of measured outgoing long-wave radiation from the NOAA-1 FPR for (A) 18 February through 16 March 1971 and (B) 10 May through 27 May 1971. The values are in tens of langleys per day.

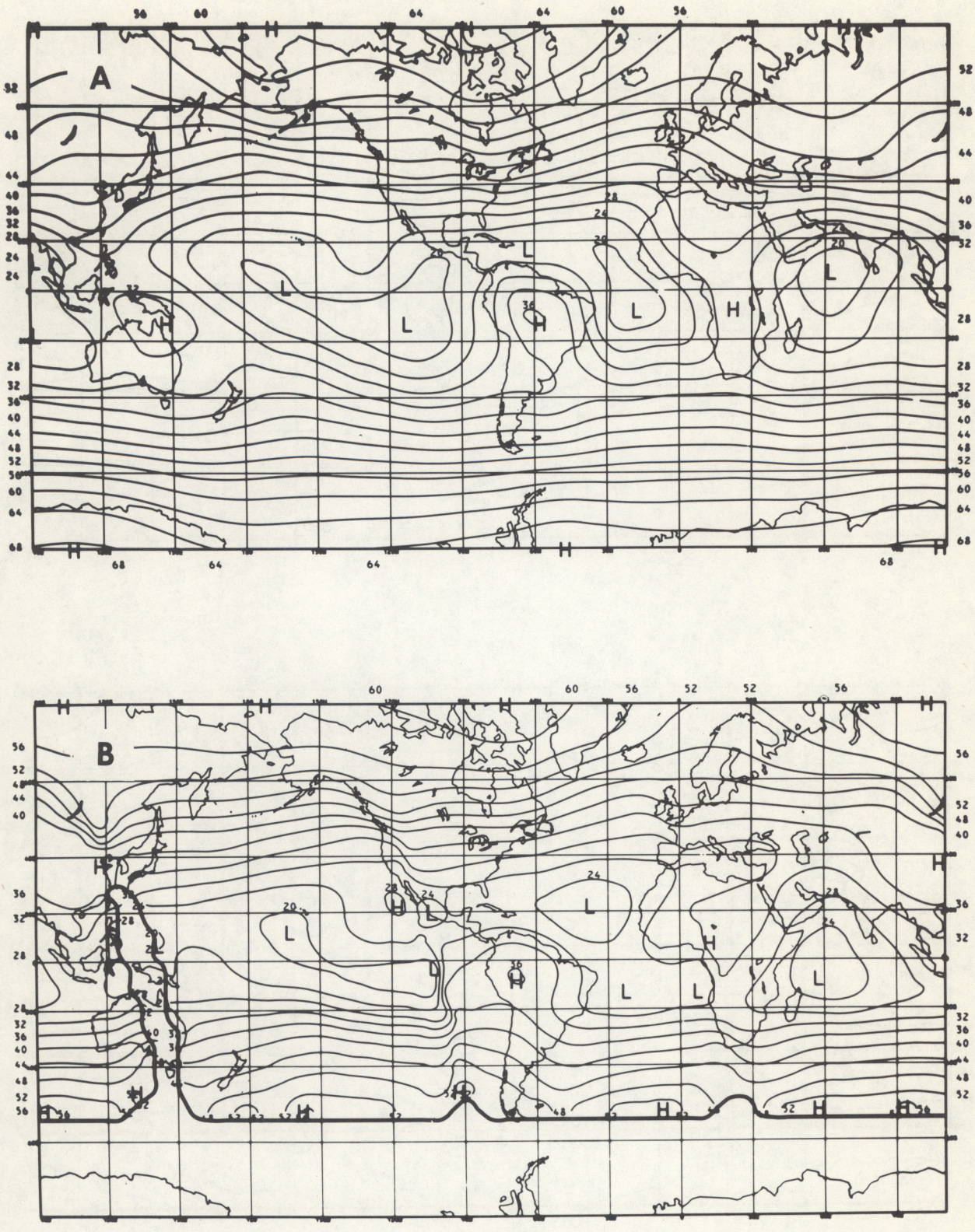

Figure 7.--Same as figure 6 except this is measured albedo. The values are in percent.

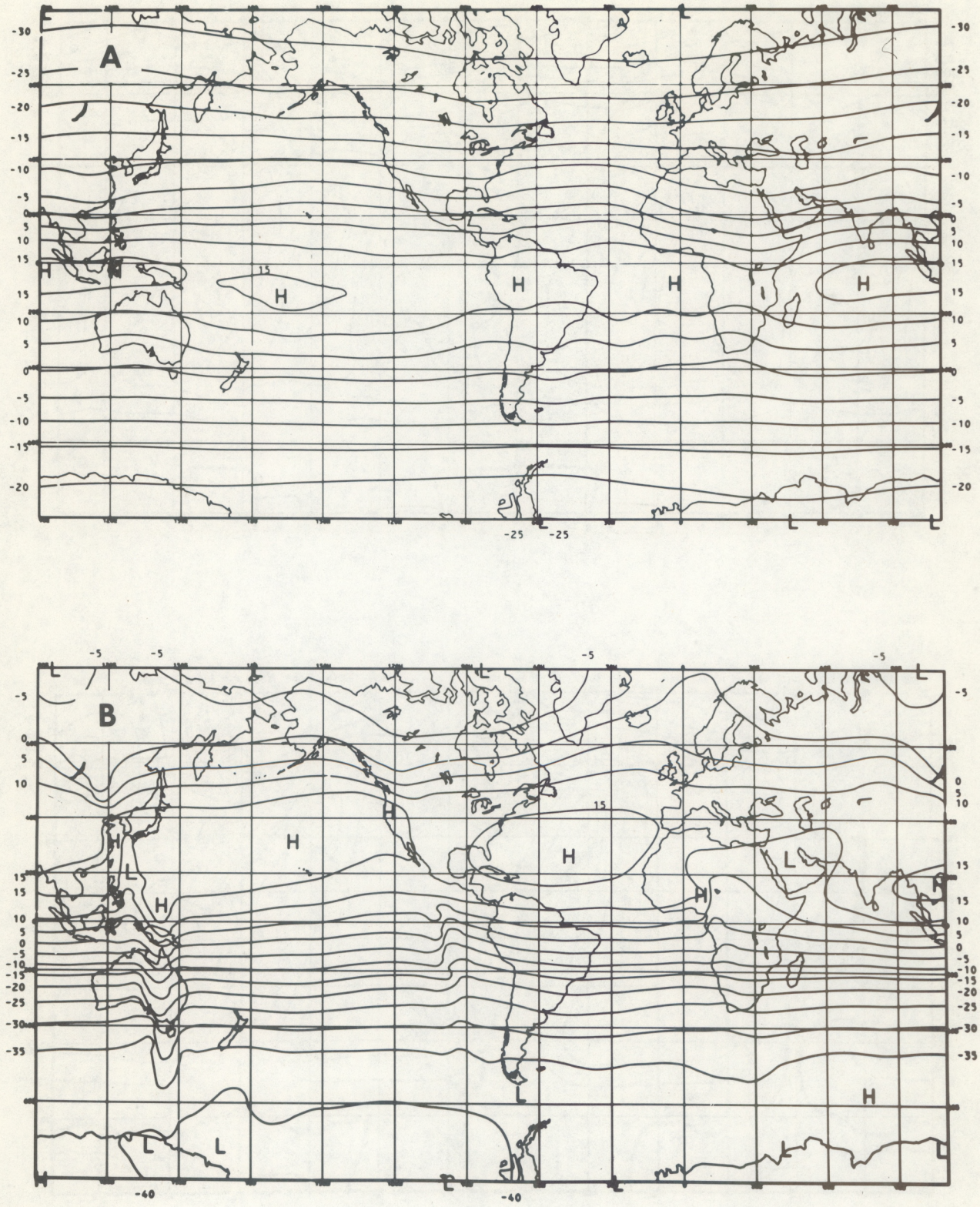

Figure 8.--Same as figure 6 except this is measured net radiation. The values are in tens of langleys per day.

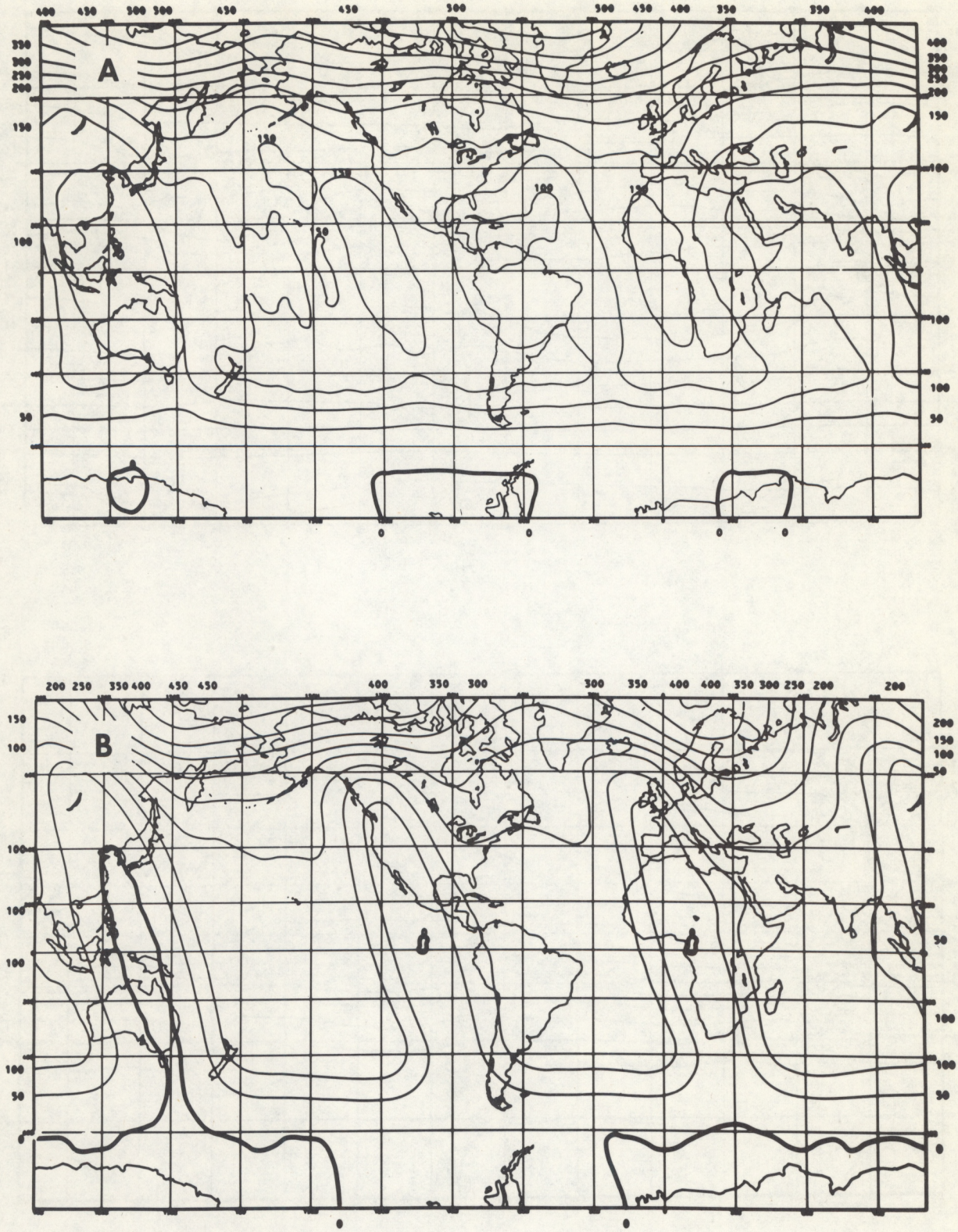

Figure 9.--Number of daytime long-wave radiation observations (A) for the ITOS-1 FPR during May 1970 and (B) for the NOAA-1 FPR during May 1971.

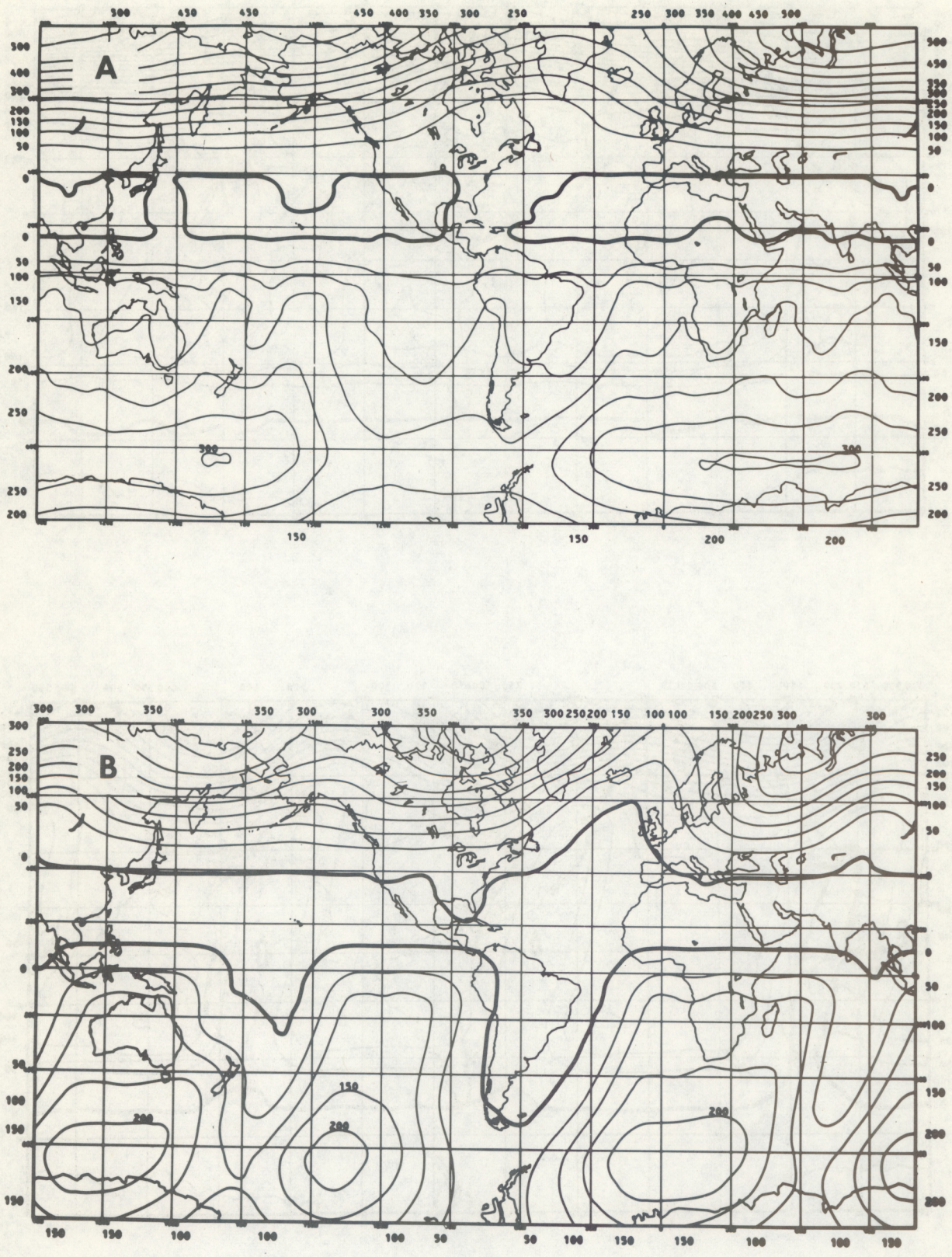

Figure 10.--Number of nighttime long-wave radiation observations (A) for the ITOS-1 FPR during May 1970 and (B) for the NOAA-1 FPR during May 1971.

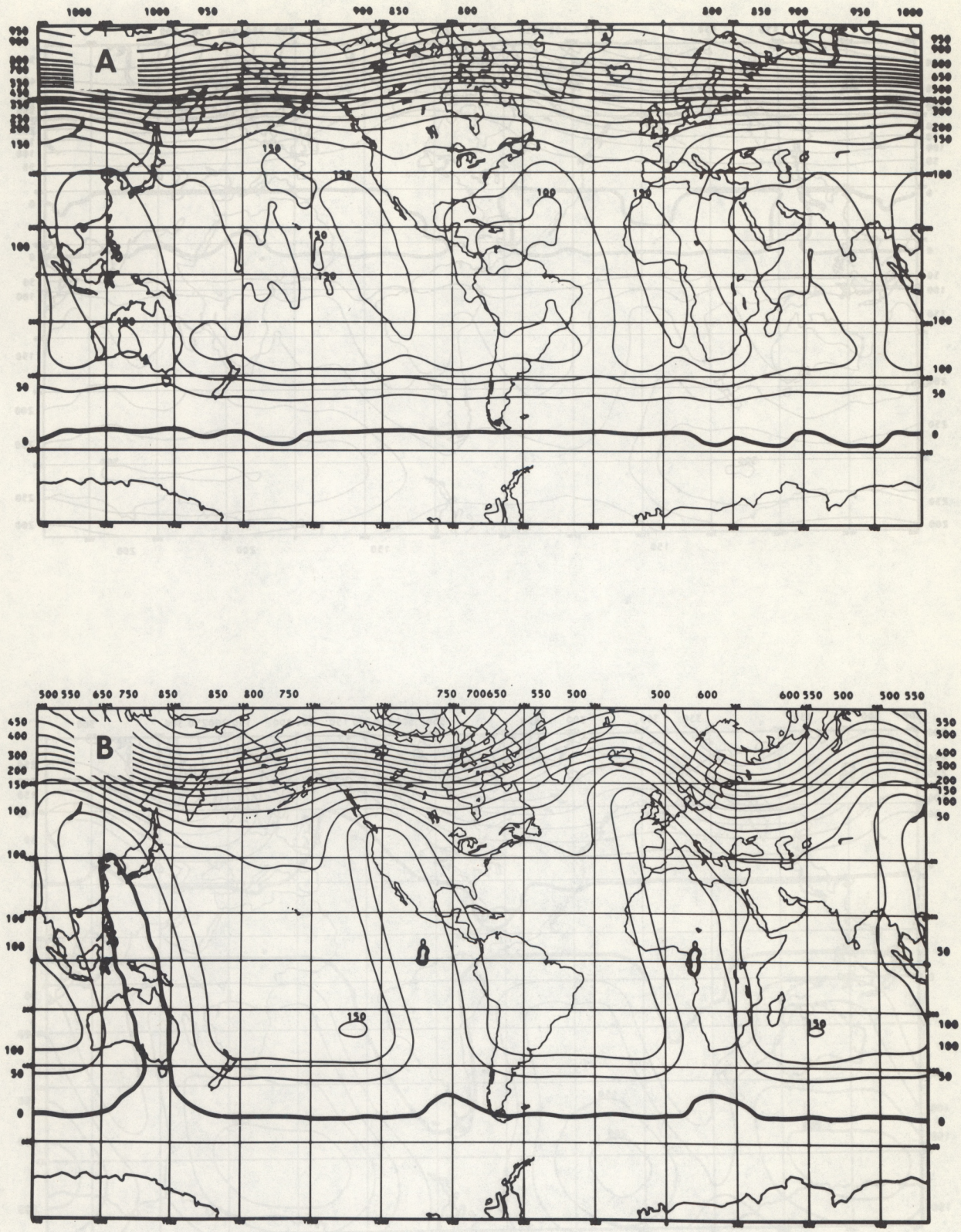

Figure 11.--Number of albedo observations (A) for the ITOS-1 FPR during May 1970 and (B) for the NOAA-1 FPR during May 1971.

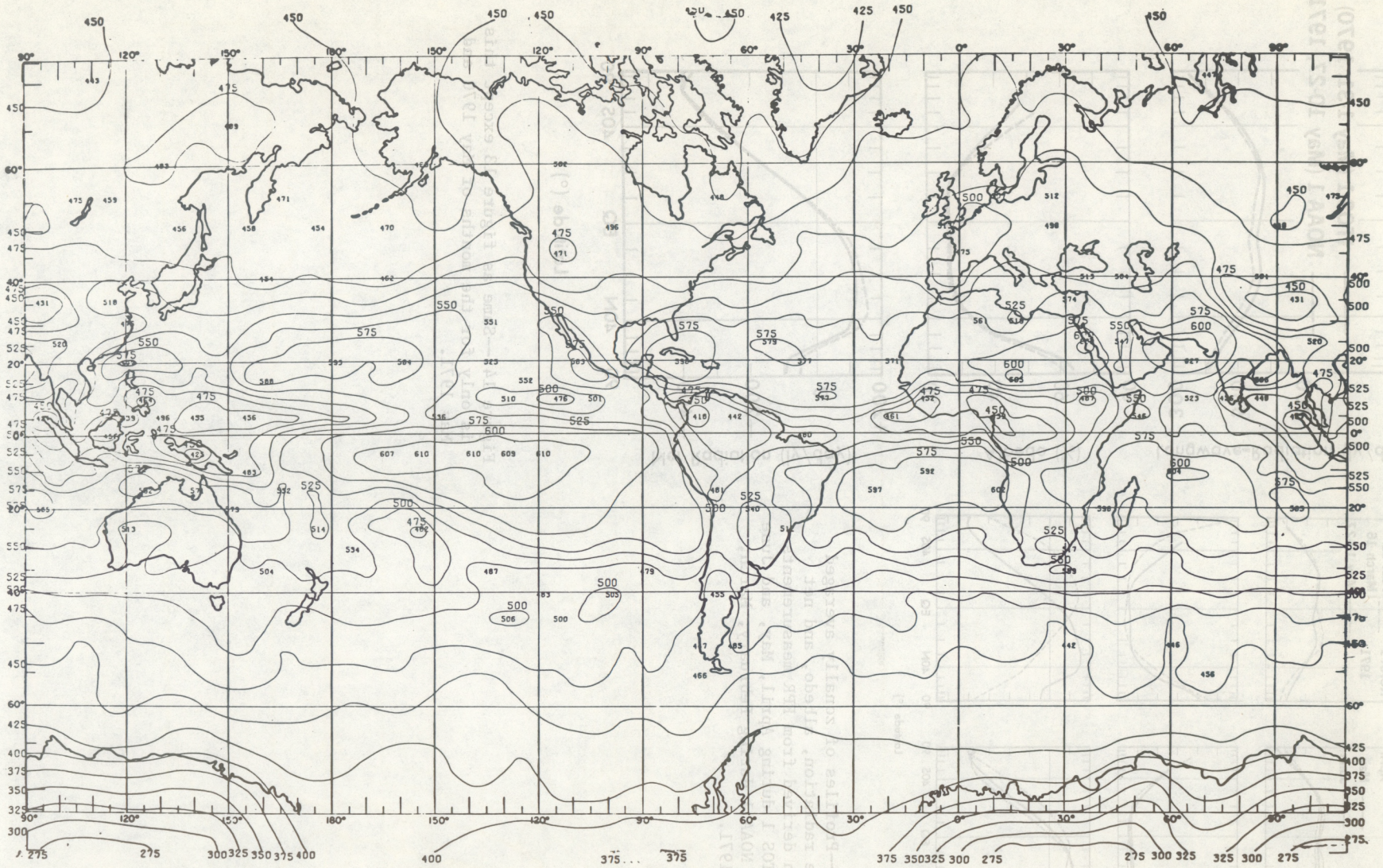

Figure 12.--Global analysis of long-wave radiation derived from the NOAA-1 Scanning Radiometer for May 1971 [provided by Winston (1975)]. The values are in langleys per day.

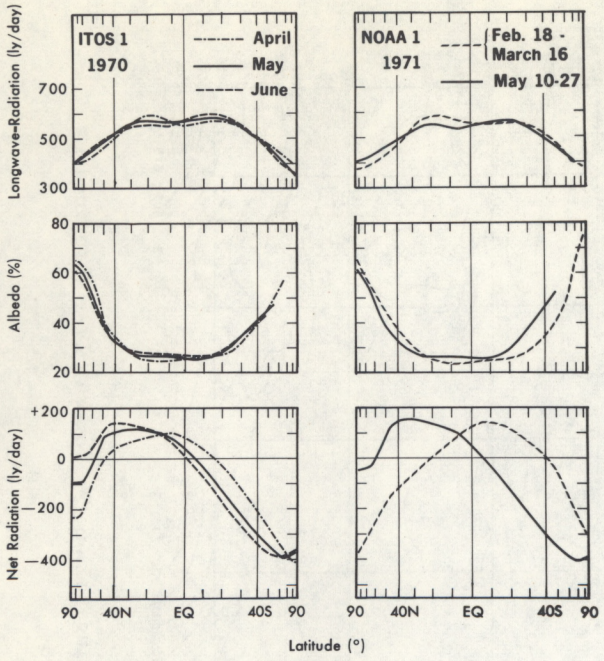

Figure 13.--Profiles of zonally averaged long-wave radiation, albedo, and net radiation derived from FPR measurements aboard ITOS 1 during April, May, and June 1970 and NOAA 1 during February, March, and May 1971.

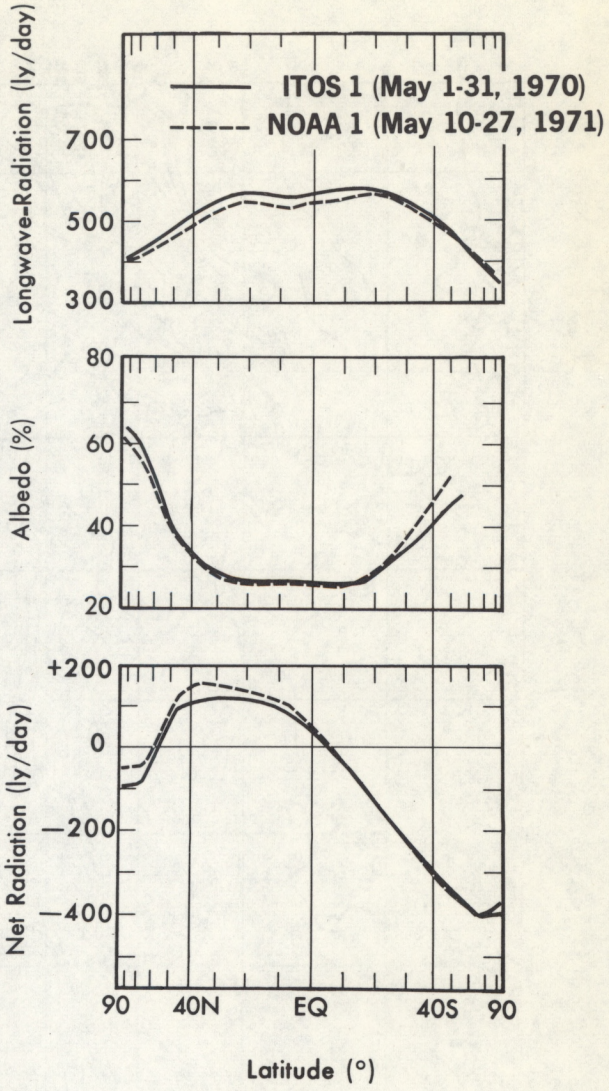

Figure 14.--Same as figure 13 except this is only for the months of May 1970 and May 1971.

(Continued from inside front cover)

NESS 50 An Examination of Tropical Cloud Clusters Using Simultaneously Observed Brightness and High Resolution Infrared Data From Satellites. Arnold Gruber, September 1973, 22 pp. (COM-73-11941/4AS)

NESS 51 SKYLAB Earth Resources Experiment Package Experiments in Oceanography and Marine Science. A. L. Grabham and John W. Sherman, III, September 1973, 72 pp. (COM 74-11740/AS)

NESS 52 Operational Products From ITOS Scanning Radiometer Data. Edward F. Conlan, October 1973, 57 pp. (COM-74-10040)

NESS 53 Catalog of Operational Satellite Products. Eugene R. Hoppe and Abraham L. Ruiz (Editors), March 1974, 91 pp. (COM-74-11339/AS)

NESS 54 A Method of Converting the SMS/GOES WEFAX Frequency (1691 MHz) to the Existing APT/WEFAX Frequency (137 MHz). John J. Nagle, April 1974, 18 pp. (COM-74-11294/AS)

NESS 55 Publications and Final Reports on Contracts and Grants, 1973. NESS, April 1974, 8 pp. (COM-74-11108/AS)

NESS 56 What Are You Looking at When You Say This Area Is a Suspect Area for Severe Weather? Arthur H. Smith, Jr., February 1974, 15 pp. (COM-74-11333/AS)

NESS 57 Nimbus-5 Sounder Data Processing System, Part I: Measurement Characteristics and Data Reduction Procedures. W.L. Smith, H. M. Woolf, P. G. Abel, C. M. Hayden, M. Chalfant, and N. Grody, June 1974, 99 pp. (COM-74-11436/AS)

NESS 58 The Role of Satellites in Snow and Ice Measurements. Donald R. Wiesnet, August 1974, 12 pp. (COM-74-11747/AS)

NESS 59 Use of Geostationary-Satellite Cloud Vectors to Estimate Tropical Cyclone Intensity. Carl. O. Erickson, September 1974, 37 pp. (COM-74-11762/AS)

NESS 60 The Operation of the NOAA Polar Satellite System. Joseph J. Fortuna and Larry N. Hambrick, November 1974, 127 pp. (COM-75-10390/AS)

NESS 61 Potential Value of Earth Satellite Measurements to Oceanographic Research in the Southern Ocean. E. Paul McClain, January 1975, 18 pp. (COM-75-10479/AS)

NESS 62 A Comparison of Infrared Imagery and Video Pictures in the Estimation of Daily Rainfall From Satellite Data. Walton A. Follansbee and Vincent J. Oliver, January 1975, 14 pp. (COM-75-10435/AS)

NESS 63 Snow Depth and Snow Extent Using VHRR Data From the NOAA-2 Satellite. David F. McGinnis, Jr., John A. Pritchard, and Donald R. Wiesnet, February 1975, 10 pp. (COM-75-10482/AS)

NESS 64 Central Processing and Analysis of Geostationary Satellite Data. Charles F. Bristor (Editor), March 1975, 155 pp. (COM-75-10853/AS)

NESS 65 Geographical Relations Between a Satellite and a Point Viewed Perpendicular to the Satellite Velocity Vector (Side Scan). Irwin Ruff and Arnold Gruber, March 1975, 14 pp. (COM-75-10678/AS)

NESS 66 A Summary of the Radiometric Technology Model of the Ocean Surface in the Microwave Region. John C. Alishouse, March 1975, 24 pp. (COM-75-10849/AS)

NESS 67 Data Collection System Geostationary Operational Environmental Satellite: Preliminary Report. Merle L. Nelson, March 1975, 48 pp. (COM-75-10679/AS)

NESS 68 Atlantic Tropical Cyclone Classifications for 1974. Donald C. Gaby, Donald R. Cochran, James B. Lushine, Samuel C. Pearce, Arthur C. Pike, and Kenneth O. Poteat, April 1975, 6 pp. (COM-75-10676/AS)

NESS 69 Publications and Final Reports on Contracts and Grants, NESS-1974. April 1975, 7 pp. (COM-75-10850/AS)

NESS 70 Dependence of VTPR Transmittance Profiles and Observed Radiances on Spectral Line Shape Parameters. Charles Braun, July 1975, 17 pp.

NESS 71 Nimbus-5 Sounder Data Processing System, Part II: Results. W. L. Smith, H. M. Woolf, C. M. Hayden, and W. C. Shen, July 1975, 102 pp.